Catal Lett (2009) 129:323–330
DOI 10.1007/s10562-009-9858-5

CO Preferential Oxidation Activity of CuO/CeO_2 Supported on Zirconium Doped Mesoporous MSU Type Silica

Elisa Moretti · Loretta Storaro · Aldo Talon · Ramón Moreno-Tost · Enrique Rodríguez-Castellón · Antonio Jiménez-López · Maurizio Lenarda

Received: 24 July 2008 / Accepted: 5 January 2009 / Published online: 23 January 2009

Abstract The activity of the $CuO–CeO_2$ couple supported on a MSU silica doped with zirconium (Si/Zr = 7), was evaluated in the preferential oxidation of CO (CO-PROX) in hydrogen-rich gas stream (1.2% CO, 1.2% O_2, 50% H_2, 0–15% CO_2, 0–10% H_2O He balance) and the catalytic performance was compared with that of $CuO–CeO_2$ supported on a pure MSU silica. The samples were characterized by X-ray powder diffraction (XRPD), N_2 physisorption at 77 K, temperature-programmed reduction (H_2-TPR) and X-ray photoelectron spectroscopy (XPS). Correlations between catalytic performances and physico–chemical properties of the materials have been made.

Keywords MSU · Mesopores · Zirconium · Ce–Cu · CO-PROX · Hydrogen production

1 Introduction

The reforming of alcohols and hydrocarbons is reasonably considered to be the most feasible method to produce large volumes of hydrogen-rich gas streams [1, 2]. Nevertheless, carbon monoxide is a typical by-product of the process and must be reduced down to ppm levels in order to use the hydrogen stream as feed for proton-exchange membrane fuel cells (PEMFCs) [3]. Among the various methods for CO removal, the selective oxidation (CO-PROX) is considered one of the most straightforward and cost effective methods to achieve acceptable CO concentrations [4, 5]. Different types of catalysts are known to be suitable for the CO-PROX process, especially those based on the $CuO–CeO_2$ couple, that is not only highly active and selective, but also very interesting from an economical point of view [6–16]. The performances of $CuO–CeO_2$ based catalysts in CO-PROX appear to be related to the peculiar synergistic redox properties in the presence of copper–ceria interfacial sites [6, 17–19]. The CO-PROX activity and selectivity appear to be improved by the presence of highly dispersed copper species on the ceria surface that favor the formation of oxygen vacancies at the copper–ceria boundaries, thus increasing the Cu reducibility [6, 17–19]. Various studies have been carried out on the system $CuO–CeO_2–ZrO_2$ [20–23], even if the role of zirconium, as well as its optimal concentration in the catalyst, is not understood completely.

Following our studies on Cu/Ce-based catalysts supported on ordered mesoporous oxides [13, 16], in this paper we tested the CO-PROX activity of $CuO–CeO_2$ supported on a structurally organized mesoporous MSU silica doped with zirconium.

E. Moretti · L. Storaro · A. Talon · M. Lenarda (✉)
INSTM UdR Venezia – Dipartimento di Chimica, Università Ca' Foscari di Venezia, Via Torino 155/B, 30172 Mestre Venezia, Italy
e-mail: lenarda@unive.it

R. Moreno-Tost · E. Rodríguez-Castellón · A. Jiménez-López
Departamento de Química Inorgánica, Cristalografía y Mineralogía (Unidad Asociada al ICP-CSIC), Facultad de Ciencias, Universidad de Málaga, Campus de Teatinos, E-29071 Málaga, Spain

2 Experiments and Methods

2.1 Reagents

All the materials used in this paper are Aldrich products and no further purification was carried out. The silicon source was a sodium silicate solution ($Na_2Si_3O_7$ with 27% SiO_2 and 14% NaOH); zirconium was incorporated via

zirconyl chloride ($ZrOCl_2 \cdot 8H_2O$). The non-ionic surfactant was polyethyleneglycol-4-ter-octylphenylether with 9–10 ethoxy groups (Triton X100). Cerium and copper were introduced as Ce $(NO_3)_3 \cdot 6H_2O$ and Cu $(NO_3)_2 \cdot 3H_2O$.

2.2 Catalysts Preparation

In this work two different mesoporous silicas were used as support: an MSU silica and a zirconium-doped MSU silica with a Si/Zr ratio of 7. The low cost syntheses of these two types of supports were already fully described elsewhere [24].

The mesoporous solids were impregnated via incipient wetness method using aqueous solutions of copper (II) and cerium (III) salts. The catalysts were prepared with a fixed cerium loading of 20 wt% and two loadings of copper (6 and 12 wt%). All samples were dried 12 h at 60 °C and then calcined at 450 °C for 4 h. The catalysts were labelled as Cu_xCe20SiZr7 and Cu_xCe20Si, where x denotes the weight percentage of copper.

2.3 Catalytic Activity Measurements

Catalytic activity tests were carried out in a laboratory flow apparatus with a fixed bed reactor operating at atmospheric pressure. The catalyst (100 mg), with a defined particle size (0.050–0.110 mm), was introduced into a tubular Pyrex glass reactor (5 mm i.d.), placed in an aluminum heating block.

Before the catalytic experiments, the sample was heated in situ at 110 °C under flowing air for 1 h. The contact time W/F was 0.18 g s cm^{-3} (where W is the catalyst weight and F the total flow rate), except when differently described. The feed consisted of 1.2% CO, 1.2% O_2 and 50% H_2 (% vol.) balanced with He (purchased from SIAD). The effect of CO_2 and H_2O were examined in separate runs with the addition of 15 vol.% CO_2 and 10 vol.% H_2O in the feed gas.

Calibration of the GC was done with a gas mixture containing 1% CO, 1% CO_2, 1% O_2 in He. When the effect of CO_2 was examined, the GC calibration was done with 15 vol.% CO_2 in He. When the effect of H_2O was evaluated, a 10 vol.% H_2O was pumped by a HPLC pump (supplied by Jasco) into the reaction stream. The gas lines were heated at 120 °C, in order to avoid water condensation after the reactor outlet. An ice-cooled water condenser was used to trap the excess of water downstream of the reactor. A HP6890 GC gas chromatograph equipped with a thermal conductivity detector was used to analyze the outlet composition. A CP Carboplot P7 column was used, with helium as carrier. The detection limit for CO was 10 ppm. The temperature was varied in the 40–190 °C range, and measurements were carried out till a steady state was achieved. Both methanation and reverse water gas shift reactions were found to be negligible in our experimental conditions. The carbon monoxide and oxygen conversions were calculated based on the CO (Eq. 1) and O_2 (Eq. 2) consumption, respectively:

$$\text{CO conversion}\,(\%) = \frac{n_{CO}^{in} - n_{CO}^{out}}{n_{CO}^{in}} \times 100 \quad (1)$$

$$O_2\,\text{conversion}\,(\%) = \frac{n_{O_2}^{in} - n_{O_2}^{out}}{n_{O_2}^{in}} \times 100. \quad (2)$$

The selectivity towards CO_2 was estimated from the oxygen mass balance as follows (Eq. 3):

$$\text{Selectivity}\,(\%) = \frac{n_{CO}^{in} - n_{CO}^{out}}{2\,(n_{O_2}^{in} - n_{O_2}^{out})} \times 100 \quad (3)$$

The excess oxygen factor (λ) is defined as (Eq. 4):

$$\lambda = 2 \times \frac{n_{O_2}^{in}}{n_{CO}^{in}}. \quad (4)$$

2.4 Characterization Techniques

N_2 adsorption–desorption measurements were performed at liquid nitrogen temperature (−196 °C) with an ASAP 2010 apparatus from Micromeritics. Before each measurement, the samples were outgassed overnight at 200 °C and 1×10^{-2} Pa. The N_2 isotherms were used to determine the specific surface areas (S.A.), using the BET equation, and the specific pore volume (V_s), calculated at $P/P_0 = 0.98$. The pore size distribution was calculated following the BJH method, assuming a cylindrical pore model.

X-ray diffraction patterns were obtained with a Siemens D5000 diffractometer, equipped with a graphite monochromator using CuKα radiation ($\lambda = 1.54184$ Å). The samples were disc shaped pressed powders. The average dimension of the crystallites was determined by Scherrer's equation.

Temperature-programmed reduction of hydrogen (H_2-TPR) was performed between room temperature and 500 °C, using a flow of Ar/H_2 (40 cm^3 min^{-1}, 10 vol.% of H_2) and a heating rate of 10 °C min^{-1}. Water produced in the reduction was eliminated by passing the gas flow through a cold finger (−80 °C). The consumption of H_2 was monitored by an on-line gas chromatograph (Shimadzu GC-14) provided with a TCD.

X-ray photoelectron spectra were collected using a Physical Electronics PHI 5700 spectrometer with non monochromatic Mg Kα radiation (300 W, 15 kV, 1,253.6 eV) for the analysis of the core level signals of O 1s, Si 2p, Zr 3d, Ce 3d and Cu 2p and with a multi-channel detector. Spectra of powdered samples were recorded with the constant pass energy values at 29.35 eV, using a 720 μm diameter analysis area. During data processing of

the XPS spectra, binding energy values were referenced to the C 1s peak (284.8 eV) from the adventitious contamination layer. The PHI ACCESS ESCA-V6.0 F software package was used for acquisition and data analysis. A Shirley-type background was subtracted from the signals. Recorded spectra were always fitted using Gauss–Lorentz curves, in order to determine the binding energy of the different element core levels more accurately. The error in BE was estimated to be ca. 0.1 eV. Short acquisition time of 10 min was used to examine C 1 s, Cu 2p and Cu LMM XPS regions in order to avoid, as much as possible, photoreduction of Cu^{2+} species. Nevertheless, a Cu^{2+} reduction in high vacuum during the analysis cannot be excluded [25].

3 Results and Discussion

3.1 Textural Parameters

The compositional and textural parameters of the supports and of the prepared catalysts are reported in Table 1.

A decrease of BET specific surface area and pore volume of the supports (SiZr7 and Si samples) was observed after the loading of ceria and copper, most probably attributable to a certain amount of pore blockage caused by the supported oxide particles.

3.2 Catalytic Activity Measurements

The composition of the inlet feed stream was initially fixed to of 1.2% CO, 1.2% O_2 and 50% H_2 (He balance) using $\lambda = 2$.

The carbon balance showed, in all the catalytic determinations, that the CO_2 production was in good agreement with the CO consumption, ruling out coking occurrence. Both methanation and reverse water gas shift reaction (rWGS) were found negligible below 200 °C in our experimental conditions.

All the samples resulted active and selective in the CO-PROX in the 40–190 °C temperature range, and the data are graphically presented in Fig. 1. No appreciable differences in the CO conversion and selectivity to CO_2 were observed as the Cu content of the catalysts varied from 6 to 12 wt% in the two SiZr7 based samples.

Both the SiZr-based catalysts resulted more active than the sample supported on pure MSU silica, in the overall temperature range. In particular, the catalyst Cu_6Ce20-SiZr7 showed the highest CO conversion values in the temperature range (40–115 °C). A selectivity loss, caused by the occurrence, above 115 °C, of the energetically favored hydrogen oxidation to water, was observed for all samples, while the CO conversion remained close or equal to 100% in the 115–165 °C range: in particular 99.1% at 115 °C and from 99.9 to 100% (considering the detection limit of 10 ppm) at 140 °C and 165 °C for both the SiZr-based catalysts, slowly decreasing with the increasing temperature.

Since carbon dioxide and water can be present in significant amounts in the reformed gases and are also reaction products, the effect of CO_2 (15 vol.%) and H_2O (10 vol.%) in the feed on the activity and selectivity of the process were also evaluated over the most representative sample ($Cu_6Ce20SiZr7$).

The influence of CO_2 addition to the inlet mixture is shown in Fig. 2. As expected, the addition causes a substantial and uniform decrease of the catalytic activity up to 165 °C; and at this temperature the conversion appears to be less affected by the presence of carbon dioxide (Fig. 2a). On the other hand, since the presence of CO_2 in the reactant feed inhibits both CO and H_2 oxidation, the selectivity of the catalyst is not significantly affected (Fig. 2b).

When both 15% CO_2 and 10% H_2O were added to the feed stream, the CO conversion drastically decreased in all the temperature range and the complete oxidation of CO was, in this case, never achieved. The highest conversion value (76%) was obtained at 190 °C.

Summarizing, $Cu_6Ce20SiZr7$ showed a good catalytic activity, resulting to be active in the whole temperature range, in particular between 115 and 140 °C. The presence of CO_2 and CO_2–H_2O in the feed stream resulted, nevertheless, detrimental for its performances.

The effect of time on stream was studied over $Cu_6Ce20SiZr7$ and $Cu_6Ce20Si$ samples (not shown). The reaction was monitored for 150 h maintaining the temperature constant at 115 °C, using an excess oxygen factor $\lambda = 2$, a $W/F = 0.18$ g s cm^{-3} and a feed of 1.2% CO, 1.2% O_2, 50% H_2 (He balance).

Table 1 Summary of the main compositional and textural properties of the catalysts

Sample	Cu (wt%)	Ceo_2 (wt%)	Si/Zr (mol/mol)	[a]S.A.$_{BET}$ (m^2 g^{-1})	[b]V_s (cm^3 g^{-1})	d_p (nm)
SiZr7	–	–	7	496	0.25	1.8
Si	–	–	–	613	0.31	1.8
$Cu_6Ce20SiZr7$	6	20	7	223	0.16	1.9
$Cu_{12}Ce20SiZr7$	12	20	7	219	0.16	2.0
$Cu_6Ce20Si$	6	20	–	291	0.16	1.8

[a] B.E.T. specific surface area

[b] Specific pore volume determined at $P/P_0 = 0.98$

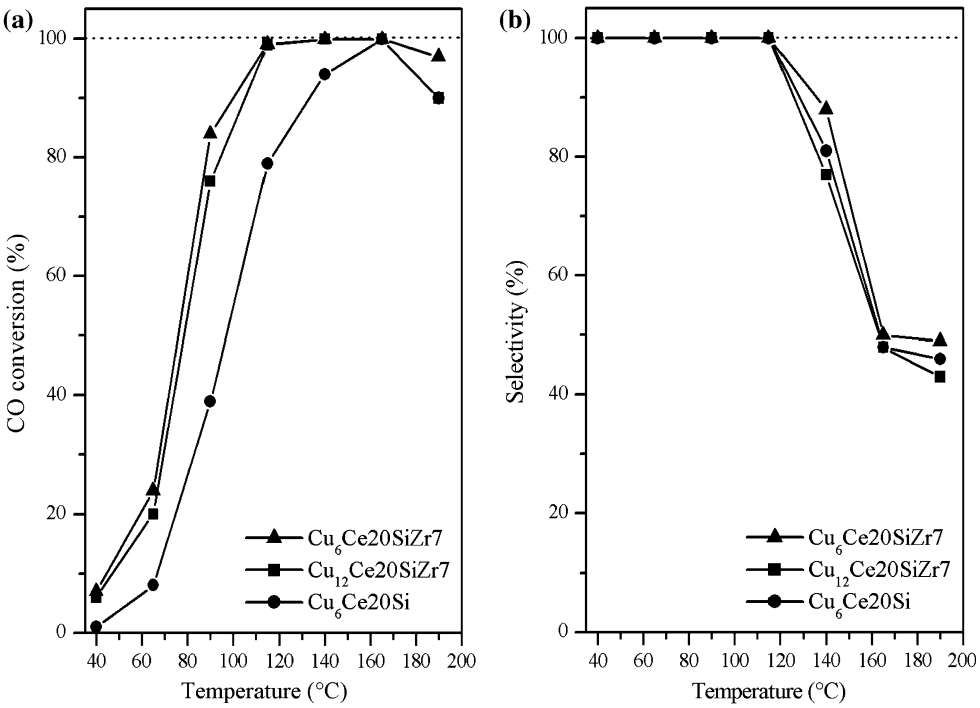

Fig. 1 Variation of the **a** CO conversion and **b** selectivity towards to CO_2 as a function of the reaction temperature obtained for the SiZr7-supported samples, with two different copper contents (6–12 wt%) and a fixed amount of ceria (20%), and for the reference sample $Cu_6Ce20Si$. Operating conditions: $\lambda = 2$; $W/F = 0.18$ g s cm^{-3}; 1.2% CO, 1.2% O_2, 50% H_2, He balance (vol.%)

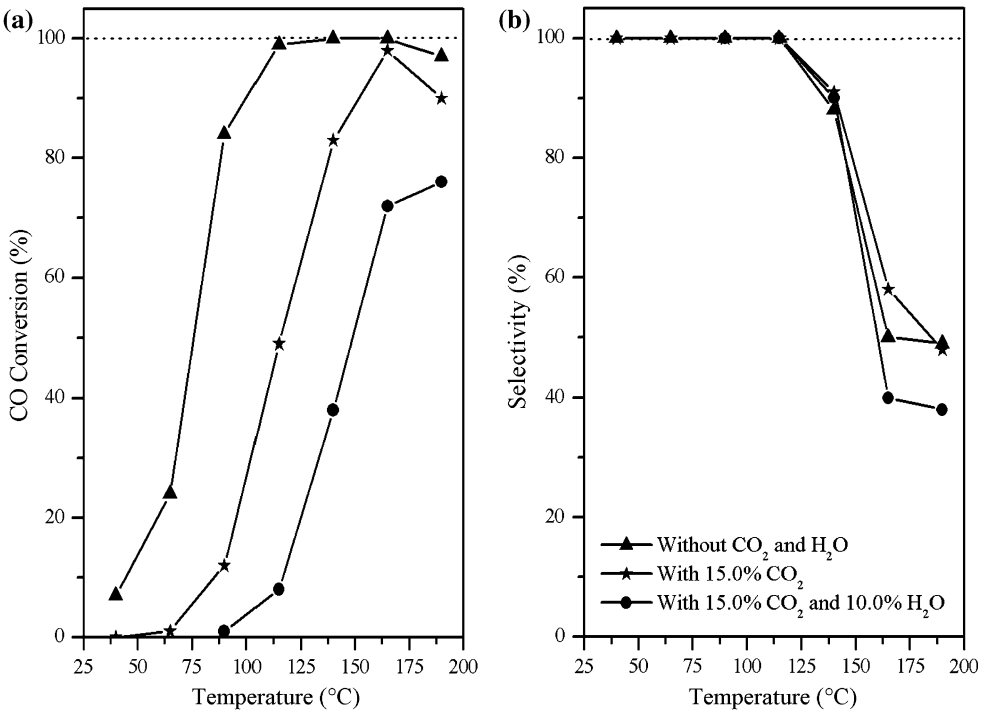

Fig. 2 Dependencies of: **a** CO conversion and **b** selectivity towards CO_2 as a function of the temperature over the catalyst $Cu_6Ce20SiZr7$, in the absence and presence of 15% CO_2 and 10% H_2O. Operating conditions: $\lambda = 2$; $W/F = 0.18$ g s cm^{-3}; 1.2% CO, 1.2% O_2, 50% H_2, 0–15% CO_2, 0–10% H_2O, He balance (vol.%)

The catalyst $Cu_6Ce20SiZr7$ showed a diminution of CO conversion from 99 to 93% within the first 5 h, remaining stable for the further operation time. In the same period (5 h), the CO conversion of the CuO–CeO_2 catalyst supported on a pure silica MSU ($Cu_6Ce20Si$) dropped from 79 to 68%.

When the effect of time on stream was tested on the catalyst $Cu_6Ce20SiZr7$ in the presence of CO_2 and H_2O at 165 °C, the conversion was observed to go from 72 to 62% within the first 3 h, slowly decreasing with the time on stream till a complete activity loss after few hours.

After the catalytic tests, all the samples resulted to maintain the same specific surface area of the fresh ones. Nevertheless, after the time on stream test in the presence of CO_2 and H_2O, the BET surface area of the sample $Cu_6Ce20SiZr7$ resulted to decrease from 223 to 180

$m^2\ g^{-1}$, suggesting a partial hydrothermal degradation of the porous structure.

3.3 X-ray Powder Diffraction (XRPD)

The XRD patterns of the Cu_xCe_20 catalysts, both as-prepared and after the PROX reaction (gas mixture: 1.2% CO, 1.2% O_2, 50% H_2, He balance), are shown in Fig. 3. No evidence for segregated crystalline cubic or monoclinic ZrO_2 was detected in the diffractograms, most probably because complete incorporation of zirconium in the tetrahedrally coordinated silica structure.

The diffraction peaks of CeO_2 (fluorite phase) at $2\theta = 28.5°$, 33.4°, 47.5° and 56.5° were observed for all the samples and the average dimension of the ceria particles, determined by the Scherrer's equation, was about 4.5 nm. The CeO_2 lattice parameters, determined for the samples containing zirconia, perfectly matched with those of the sample supported on pure MSU silica. The diffraction peaks assigned to CuO (tenorite phase) at $2\theta = 35.5°$ and 38.7° were identified only in the sample containing 12 wt% of Cu (Fig. 3b) and the average dimension of the CuO particles was 65.0 nm.

The lacking of the CuO phase in the XRD patterns of the catalysts with 6 wt% of copper may be due both to the presence of a too small amount of oxide and to the uniform distribution of Cu^{2+} species and clusters on the support. Moreover, it is known that the ceria favours the increase of copper dispersion, reducing the particle size of copper [26].

A sharp and intense diffraction peak at 43.5° attributable to a metallic Cu phase was detected in the diffractogram of the $Cu_{12}Ce20SiZr7$ catalyst measured after reaction, evidencing the presence of large Cu crystallites. No modifications in the X-ray profile were observed for $Cu_6Ce20SiZr7$, after the effect of time on stream in the presence of CO_2 and H_2O.

3.4 Temperature-Programmed Reduction of Hydrogen (H_2-TPR)

H_2-TPR profiles of Cu_xCe_20-catalysts are shown in Fig. 4. As known from the literature [20], pure zirconia cannot be reduced in hydrogen below 930 °C. On the other hand ceria does not show any reduction peak below 500 °C [13]. The reduction of copper oxide supported on CeO_2 [9, 27, 28] and CeO_2–ZrO_2 [20, 22] was observed to start above 100 °C, while pure CuO is reduced above 250 °C. CuO supported on zirconium containing mesoporous silica was found to be reduced at lower temperature than bulk CuO [29]. Ceria promotion of the copper species reduction was reported by several authors [9, 20, 22, 27, 28, 30, 31] and the reducibility was found to increase with the decreasing size of CuO particles [9, 32]. Avgouropoulos [9, 27], studying the reduction of CuO supported on ceria,

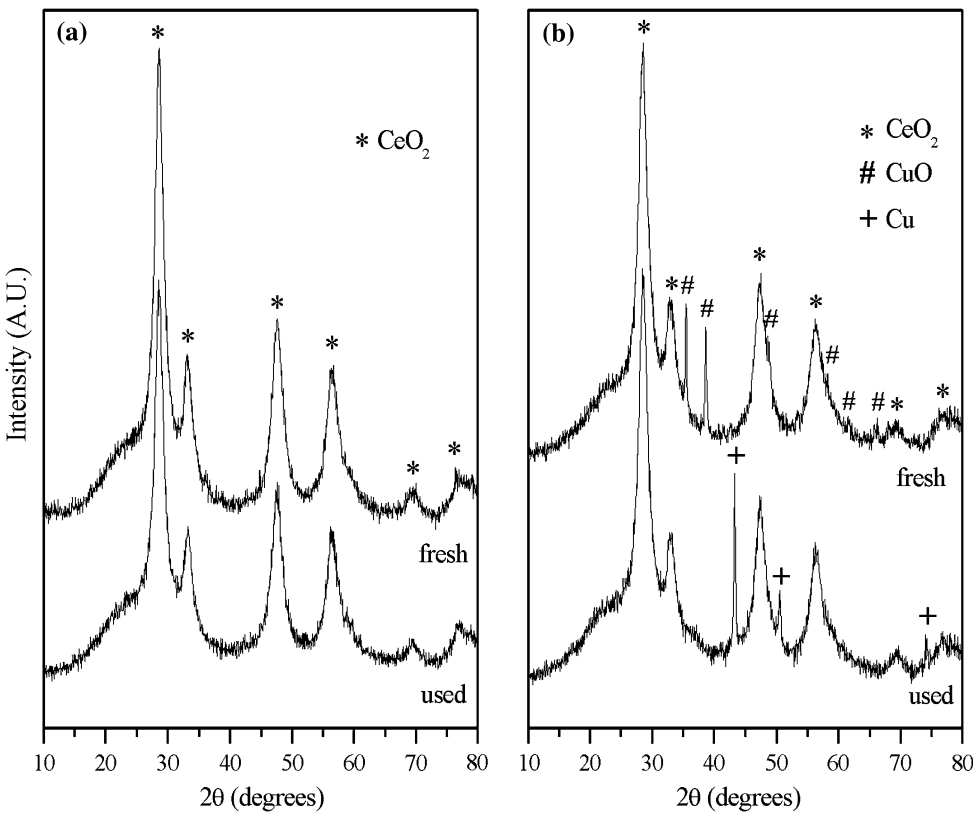

Fig. 3 X-ray powder diffraction profiles before and after the catalytic test for the samples: **a** $Cu_6Ce20SiZr7$ and **b** $Cu_{12}Ce20SiZr7$. Operating conditions for the mentioned catalytic test: 1.2% CO, 1.2% O_2, 50% H_2, He balance, $W/F = 0.18$ g s cm^{-3}, $\lambda = 2$

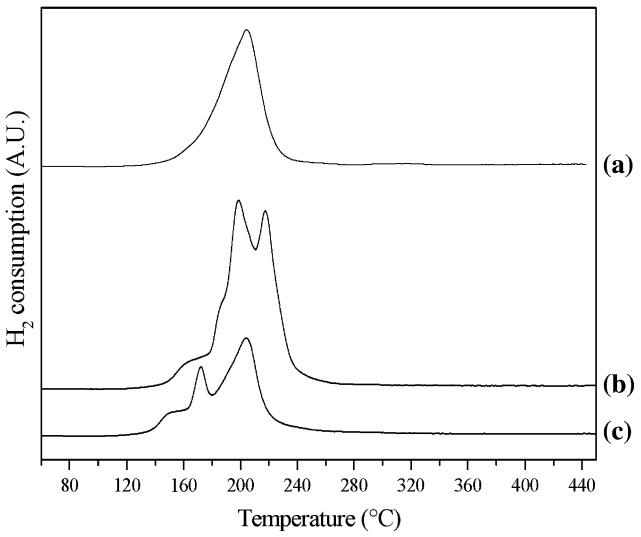

Fig. 4 H_2-TPR profiles of the catalysts: **a** $Cu_6Ce20Si$ **b** $Cu_{12}Ce20SiZr7$ **c** $Cu_6Ce20SiZr7$

attributed a peak at ca. 170 °C to the reduction of highly dispersed CuO strongly interacting with the ceria surface and two peaks at 220 °C and 255 °C to the reduction of larger CuO particles weakly interacting with ceria. Dong [22] observed a broad reduction peak with a shoulder at low temperature, attributable to the reduction of highly dispersed copper oxide species interacting with ceria, and a peak at higher temperature attributable to the reduction of bulk-like CuO. Ratnasamy [20] showed that the reducibility of CuO on different supports increases in the order $CuO–ZrO_2 \leq CuO–CeO_2–ZrO_2 < CuO–CeO_2$.

Luo [30] studied the reduction of $CuO–CeO_2$ catalysts and observed a two-step reduction profile indicating the existence of two CuO species. The low temperature peak was associated to small CuO particles finely dispersed and interacting with ceria, while the higher temperature one was assigned to the reduction of larger CuO particles.

The TPR profiles of the two samples of SiZr7-based catalysts show a shoulder and two peaks with maxima at 151 °C (shoulder), 172 °C and 204 °C for the $Cu_6Ce20SiZr7$ sample and 161 °C (shoulder), 198 °C and 217 °C for the $Cu_{12}Ce20SiZr7$ sample. According to literature data [20, 22], the TPR profiles of the SiZr7-based catalysts show the presence of two types of well dispersed Cu species strongly interacting with the Ce20SiZr7 surface, corresponding to the reduction peaks, respectively, at 151 and 172 °C for $Cu_6Ce20SiZr7$ and 161 and 198 °C for $Cu_{12}Ce20$ SiZr7. The peaks above 200 °C were attributed, for both samples, to the reduction of bulk-like CuO particles. Copper species in the $Cu_6Ce20SiZr7$ sample are reduced at lower temperature than those present in the $Cu_{12}Ce20SiZr7$ sample that contains a larger amount of Cu. Because it is known that the reduction temperature of CuO particles increases with the increase of their dimensions, it appears that the higher copper loading in the $Cu_{12}Ce20SiZr7$ sample, results mainly in the formation of bigger CuO particles, weakly interacting with ceria and therefore reducible at higher temperature. The catalyst based on pure silica shows a consumption peak of H_2 centred at 204 °C with a shoulder at 192 °C. The shoulder at lower temperature is ascribed to copper oxide interacting with ceria and the peak at higher temperature to the CuO particles weakly interacting with ceria [33].

3.5 X-ray Photoelectron Spectroscopy (XPS)

Catalyst surface composition, before and after the catalytic tests (gas mixture: 1.2% CO, 1.2% O_2, 50% H_2, He balance), was studied by means of XPS. The Cu 2*p* core level of the catalysts present a complex spectrum that is shown in Fig. 5a–b. The $CuO–CeO_2$ system has been studied by many authors [9, 34–36], that identified different copper species. Thus, Avgouropoulos [9] showed that Cu could be present both as Cu^{2+} and Cu^{1+} species. Kundakovic [34] detected CuO particles and small clusters of copper, at low copper loading, which did not show the CuO spectroscopic characteristics. Zou [35] noted that, before being used in the selective oxidation of CO (CO-PROX), Cu (10 wt%)–CeO_2 was composed by a mixture of both Cu^{2+} and Cu^{+}. Xiaoyuan [36] also showed the simultaneous existence of Cu^{2+} and Cu^{1+} for Cu (5 wt%)–CeO_2 catalyst, due to the strong interaction between the redox couple (Ce^{4+}/Ce^{3+}) and CuO.

The XPS spectra of $Cu_6Ce20SiZr7$ and $Cu_{12}Ce20SiZr7$ fresh samples show in the Cu 2*p* region peaks at 932.5 and 934.4 eV, respectively. These two peaks, according with the literature [27] could be ascribed to the presence of CuO particles (peak at higher binding energy) and reduced copper species or small clusters of copper (peak at lower BE) formed by the strong interaction between copper and ceria. This interaction was already showed by H_2-TPR profiles (Fig. 4), which exhibited a main peak with a shoulder at low temperature, being this shoulder due to a copper species close interacting with ceria. When the copper loading increased (Fig. 5b), the peak at high BE increased its intensity, pointing out that the predominant copper species are CuO particles.

After reaction, the two catalysts showed a similar behaviour: the Cu 2*p* core level signal can be decomposed into two peaks related to CuO particles whose intensity decreased after the catalytic tests, as the peak related to copper species strongly interacting with ceria is shifted to lower BE and may be ascribed to Cu^0, the presence of which was detected in the XRD patterns of the catalysts after catalytic reaction (Fig. 3). The peak corresponding to CuO particles disappears in the catalytic conditions for the $Cu_{12}Ce20SiZr7$ catalyst.

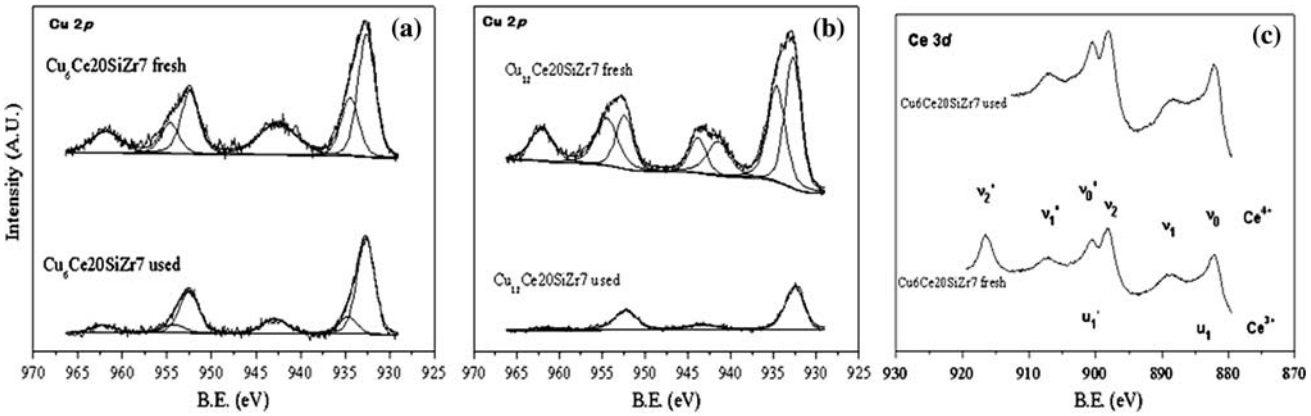

Fig. 5 **a** Cu 2*p* photoelectron profiles of $Cu_6Ce20SiZr7$ fresh and used; **b** Cu 2*p* XPS spectra of $Cu_{12}Ce20SiZr7$ fresh and used; **c** core level Ce 3*d* spectra of $Cu_6Ce20SiZr7$ fresh and used. Operating conditions of the mentioned catalytic test: 1.2% CO, 1.2% O_2, 50% H_2, He balance, $W/F = 0.18$ g s cm^{-3}, $\lambda = 2$

This is demonstrated by the observed decrease of the intensity ratio of the shake-up satellite and the intensity of the Cu $2p_{3/2}$ peak (ICu_{sat}/ICu_{2p}). In Table 2 the (ICu_{sat}/ICu_{2p}) ratios for the fresh and used catalysts are compiled and they appear to be always lower for the used catalysts. Moreover these values are in the range for CuO (0.55) and Cu^0 (0) [27].

The core level Ce 3*d* signal of ceria is typically composed [36] of six peaks v_0, v_1, and v_2 (Ce $3d_{5/2}$) and v_0', v_1', and v_2' (Ce $3d_{3/2}$) and corresponds to Ce^{4+} 3*d* final states. The low binding energy doublet v_1/v_1' at 888.9 and 907.5 eV originated from the state Ce(IV)$3d^9 4f^1 O2p^5$, the doublet v_0/v_0' at 882.3 and 901.0 eV from the state Ce(IV)$3d^9 4f^2 O2p^4$, and the doublet v_2/v_2' at 898.2 and 916.8 eV corresponds to the final state Ce(IV)$3d^9 4f^0 O2p^6$. Ce^{3+} oxide species present a doublet u_0/u_0' at 880.5 and 898.8 eV assigned to the final state Ce(III)$3d^9 4f^1 O2p^6$, and a doublet u_1/u_1' originated from the final state Ce(III)$3d^9 4f^2 O2p^5$ at 885.7 and 904.1 eV.

In Fig. 5c, the core level Ce 3*d* spectra of the fresh and used $Cu_6Ce20SiZr7$ samples are presented, showing, before catalytic tests, only the presence of Ce^{4+}. After CO-PROX reaction, the intensity of the shoulders corresponding to the simultaneous presence of Ce^{3+} also increases. The rest of catalysts present a similar behaviour as fresh $Cu_6Ce20SiZr7$.

4 Conclusions

The CO-PROX reaction was preliminarily tested on two $CuO–CeO_2$ samples with different copper loadings supported on a structurally organized mesoporous MSU silica doped with zirconium (Si/Zr = 7) and their catalytic performances were compared with that of $CuO–CeO_2$ supported on a pure MSU silica. Both zirconia-containing samples showed good values of CO conversion and selectivity, in particular in the 115–140 °C temperature range, that is technologically interesting for PEM fuel cells. No appreciable differences were observed as the Cu content of the catalysts varied from 6 to 12 wt%. In fact the exceeding copper appears to be present as bulk CuO species which are reduced to metallic Cu in the reaction environment (as shown by XRPD measurements), that is known to be not active in the CO-PROX.

When 15% CO_2 or 15% CO_2–10% H_2O were added to the feed stream, the CO conversion drastically decreased and, in the latter case, the complete oxidation of CO cannot be achieved. XRPD analysis, performed on the material after this last catalytic test, did not evidence any significant modification, while the BET specific surface area decreased suggesting a partial degradation of the porous structure, probably generated by the thermal treatment in the presence of a relevant water amount.

Table 2 Surface atomic ratios from X-ray photoelectron spectroscopy of the SiZr-based catalysts before and after the CO-PROX reaction

Sample	O %	Si %	Cu %	Zr %	Ce %	Cu/Ce	Cu/Si	Ce/Si	I Cu $2p_{3/2}$/I Cu sat
$Cu_6Ce20SiZr7$ fresh	69.69	14.06	6.98	1.05	8.22	0.85	0.496	0.585	0.40
$Cu_6Ce20SiZr7$ used	69.35	18.89	4.83	1.72	5.21	0.93	0.256	0.276	0.17
$Cu_{12}Ce20SiZr7$ fresh	68.68	19.93	4.24	1.63	5.53	0.7	0.213	0.277	0.40
$Cu_{12}Ce20SiZr7$ used	69.67	13.06	9.20	1.22	6.84	1.34	0.704	0.524	0.21

As evidenced by H_2-TPR and XPS data, reduced copper species or small clusters of copper strongly interacting with ceria, which are the species active in the PROX reaction, prevail in the ZrO_2-containing MSU samples. The relatively high density of defects of the zirconia-doped MSU silica most probably favors the formation, even at quite high metal loadings, of well dispersed copper particles in close contact with ceria.

Acknowledgments The Ministero dell'Università e Ricerca (MiUR-PRIN 2006) is gratefully acknowledged for financial support by the Italian authors. The Spanish authors thanks the Project NAN2004-09267-C03-01 (Ministerio de Educacion y Ciencia, Spain).

References

1. Song C (2002) Catal Today 77:17
2. Navarro RM, Peña MA, Fierro JLG (2007) Chem Rev 107:3952
3. Farrauto R, Hwang S, Shore L, Ruettinger W, Lampert J, Giroux T, Liu Y, Ilinich O (2003) Annu Rev Mater Res 33:1
4. Wang JB, Lin S, Huang T (2002) Appl Catal A 232:107
5. Kim WB, Voitl T, Rodríguez-Rivera GJ, Evans ST, Dumesic JA (2005) Angew Chem Int Ed 44:778
6. Kim DH, Cha JE (2003) Catal Lett 86:107
7. Cheekatamarla PK, Epling WS, Lane AM (2005) J Power Sources 147:178
8. Martínez-Arias A, Hungría AB, Fernández-García M, Conesa JC, Munuera G (2005) J Power Sources 151:32
9. Avgouropoulos G, Ioannides T, Matralis H (2005) Appl Catal B 56:87 (and references therein)
10. Marbán G, Fuertes AB (2005) Appl Catal B 57:43
11. Martínez-Arias A, Hungría AB, Munuera G, Gamarra D (2006) Appl Catal B 65:207
12. Caputo T, Pirone R, Russo G (2006) Kinet Catal 47:761
13. Moretti E, Lenarda M, Storaro L, Talon A, Frattini R, Polizzi S, Rodríguez-Castellón E, Jiménez-López A (2007) Appl Catal B 72:149 (and references therein)
14. Liu Z, Zhou R, Zheng X (2007) J Mol Catal A Chem 267:137
15. Lippits MJ, Gluhoi AC, Nieuwenhuiys BE (2007) Topic Catal 44:159
16. Moretti E, Lenarda M, Storaro L, Talon A, Montanari T, Busca G, Rodríguez-Castellón E, Jiménez-López A, Turco M, Bagnasco G, Frattini R (2008) Appl Catal A 335
17. Martínez-Arias A, Fernández-García M, Gálvez O, Coronado JM, Anderson JA, Conesa JC, Soria J, Munuera G (2000) J Catal 195:207
18. Harrison PG, Ball IK, Azelee W, Daniell W, Goldfarb D (2000) Chem Mater 12:3715
19. Gamarra D, Hornés A, Koppány Z, Schay Z, Munuera G, Soria J, Martínez-Arias A (2007) J Power Sources 169:110 (and references therein)
20. Ratnasamy P, Srinivas D, Satyanarayana CVV, Manikandan P, Senthil Kumaran RS, Sachin M, Shetti VN (2004) J Catal 221:455
21. Manzoli M, Di Monte R, Boccuzzi F, Coluccia S, Kaspar J (2005) Appl Catal B 61:192
22. Dong X-F, Zou H-B, Lin W-M (2006) Int J Hydrogen Energy 31:2337
23. Chen Y-Z, Liaw B-J, Chen H-C (2006) Int J Hydrogen Energy 31:427
24. Infantes-Molina A, Mérida-Robles J, Maireles-Torres P, Finocchio E, Busca G, Rodríguez-Castellón E, Fierro JLG, Jiménez-López A (2004) Microp Mesop Mater 75:23
25. Poulston S, Parlett PM, Stone P, Bowker M (1996) Surf Interface Anal 24:811
26. Fernández-García M, Gómez Rebollo E, Guerrero Ruiz A, Conesa JC, Soria J (1997) J Catal 172:146
27. Avgouropoulos G, Ioannides T (2003) Appl Catal A 244:155
28. Bera P, Priolkar KR, Sarode PR, Hegde MS, Emura S, Kumashiro R, Lalla NP (2002) Chem Mater 14:3591
29. Moreno-Tost R, Santamaría-González J, Maireles-Torres P, Rodríguez-Castellón E, Jiménez-López A (2002) Catal Lett 82:205
30. Luo M-F, Zhong Y-J, Yuan X-X, Zheng X-M (1997) Appl Catal A 162:121
31. Xiaoyuan J, Guanglie L, Renxian Z, Jianxin M, Yu C, Xiaoming Z (2001) Appl Surf Sci 173:208
32. Qiu L, Liu F, Zhao L, Ma Y, Yao J (2006) Appl Surf Sci 252:4931
33. Jones A, McNicol BD (1986) Temperature-programmed reduction for solid materials characterization. M. Dekker Inc., NewYork
34. Kundakovic LJ, Flytzani-Stephanopoulos M (1998) Appl Catal A 171:13
35. Zou H, Dong X, Lin W (2006) Appl Surf Sci 253:2893
36. Xiaoyuan J, Liping L, Yingxu C, Xiaoming Z (2003) J Mol Catal A 197:193